CONF-8810118--9

Workshop on Momentum Distributions - Ed R.S. Ivey & P. Sokol (Plenum)

# MOMENTUM DISTRIBUTIONS IN LIQUID HELIUM

CONF-8810118--9

DE89 014679

P.E. Sokol

Department of Physics
The Pennsylvania State University
University Park, PA 16802

T.R. Sosnick† and W.M. Snow‡

Intense Pulsed Neutron Source and Materials Science Division
Argonne National Laboratory
Argonne, IL 60439

## INTRODUCTION

Helium is unique among the elements in that it remains liquid even at T=0 due to its light mass and weak attractive interactions. Consequently, the zero point motion is very large and the atomic wavefunctions of the helium atoms have a large overlap. This leads to many interesting properties in the liquid that depend on the quantum mechanical statistics of the particles. For example, the superfluid properties of liquid $^4$He are a consequence of the Bose statistics obeyed by $^4$He atoms. Alternately, the Fermi liquid behavior and the low temperature superfluid phase of liquid $^3$He are a direct consequence of the Fermi statistics obeyed by $^3$He atoms.

Liquid $^4$He has been extensively studied due to its unique properties and we shall concentrate on it in this review. The liquid does not form, at atmospheric pressure, until nearly 4 K, illustrating the weakness of the attractive interactions. The properties of the liquid at high temperature, near liquification, are similar to conventional liquids. However, as the temperature is lowered a transition from the high temperature phase ( Helium I ) to a new phase ( Helium II ) occurs at $\approx$ 2.2 K. This transition is marked by a sharp feature in the specific heat — the famous $\lambda$ transition — and by a change in the thermal and mass transport properties. In this new phase the liquid appears to develop a component that flows without viscosity and has infinite thermal conductivity — the superfluid — and the phase is often called the superfluid phase. Phenomenologically, this new phase can be described by the 'two-fluid' model, where the liquid is composed of two interpenetrating liquids, a superfluid component that approaches unity at T=0 and a normal component that is responsible for dissipation.

---

† Present address:Biophysics Division, Los Alamos National Laboratory, Los Alamos, NM 87545

‡ Permanent address: Lyman Laboratory of Physics, Harvard University, Cambridge, MA 02138

The appearance of the superfluid phase, with its unique macroscopic properties, and the success of the 'two-fluid' model in describing the transport properties are intimately linked to the Bose statistics obeyed by $^4$He atoms. London[1] first suggested that the underlying microscopic cause for the spectacular macroscopic effects observed in the superfluid phase was due to the appearance of a Bose condensate, a macroscopic occupation of a single quantum state. Since this insightful suggestion there has been extensive theoretical work and the idea of a Bose condensate, or a broken Bose symmetry, has remained central to our understanding of the superfluid phase.

The most direct signature of the Bose condensate is in the single particle momentum distribution $n(p)$. In the normal liquid the momentum distribution has a broad Gaussian shape, as predicted for classical systems, with a width determined by the quantum zero point motion. In the superfluid phase a new feature appears, the Bose condensate. The condensate appears as a $\delta$-function singularity in $n(p)$ with an intensity proportional to $n_0$, the condensate fraction.

There has been extensive experimental work attempting to verify the existence of the condensate. Hohenberg and Platzman[2] originally suggested that inelastic neutron scattering at high momentum transfers $Q$, where the Impulse Approximation IA can be used to directly relate the observed scattering to $n(p)$, could provide a means of directly observing the condensate. There is now a long history of attempts to directly verify the existence of the Bose condensate.[3] Unfortunately, despite many years of experimental work, a direct observation of the condensate has still not occurred.

Most of the previous experimental studies aimed at determining the momentum distribution have been carried out at reactor based neutron sources.[5-12] These measurements, due to the thermal spectrum of neutrons available from reactors, are limited to $Q$'s below 10-12 Å$^{-1}$, although through some herculean efforts[4] there have been measurements at somewhat larger $Q$'s. Unfortunately, at these $Q$'s deviations from the Impulse Approximation are quite apparent and have prevented a direct observation of the condensate. Even when approximate methods are used to correct for these deviations, significant differences between the theoretical predictions for the momentum distribution and the experimental results exist.

In this review we will not attempt to comprehensively cover the great body of past work in this area. This has been very throughly and ably covered in several recent review articles.[13,14,4] Instead, we will concentrate on recent experimental studies that utilize the large flux of high energy neutrons available at spallation neutron sources. These sources, which have become available only recently, have made it possible to make detailed measurements at large enough momentum transfers that the conditions for the Impulse Approximation are approximately satisfied. While deviations from the IA are still present at these higher $Q$'s, they are more amenable to theoretical treatment and detailed predictions are available. Thus, even though no distinct condensate peak is observed, for the first time excellent agreement with the theoretical predictions for $n(p)$ can be obtained.

## REVIEW

We begin with a brief review of the current theoretical studies of the momentum distribution in liquid $^4$He. Complete and detailed descriptions of the theoretical work are presented elsewhere in these proceedings.[15,16,17,18] Therefore, we shall limit our discussion to the most recent examples.

Liquid helium provides a very challenging system for theoretical studies. The attractive part of the helium potential is quite weak, as evidenced by the stability of the liquid even at T=0. This leads to a large overlap of the atomic wavefunctions which make quantum statistics an important factor in determining the properties of the ground state. However, while the attractive interactions are quite small the hard core repulsion between atoms is very large. This makes liquid helium a very

strongly interacting system, in some sense even more strongly interacting than nuclear matter.[15] Therefore, it has been extremely difficult to develop a comprehensive microscopic theory of the dense liquid phase using perturbative techniques.[19] Some specific results can be obtained using analytic techniques. For example, a major success of these theories is the prediction of the relationship[20] between the broken Bose symmetry that characterizes the ground state when a condensate is present and the superfluid properties. In general, though, it has not been possible to develop a comprehensive microscopic theory of the ground or excited states of the liquid.

In view of the difficulty associated with analytic theories, the most detailed and comprehensive results for $n(p)$ have come from numerical calculations. Variational[16] and Greens Function Monte Carlo (GFMC)[18] techniques have been applied extensively to calculating the properties of the ground state at T=0. These first principles calculations, using realistic potentials, have obtained good agreement with several measured properties for the ground state of the liquid, such as the total energy and static structure of the liquid.

The most prominent feature in the ground state $n(p)$ is the appearance of a condensate, a $\delta$ function singularity at $p = 0$. Fig. 1 shows two recent calculations of $n(p)$ in the ground state, using GFMC[21] and variational[22] techniques. Both calculations show a condensate $\delta$ function (not visible in the variational calculation). The intensity in this $\delta$ function, which is known as the condensate fraction $n_0$, is $\approx 9$ % of the total intensity.

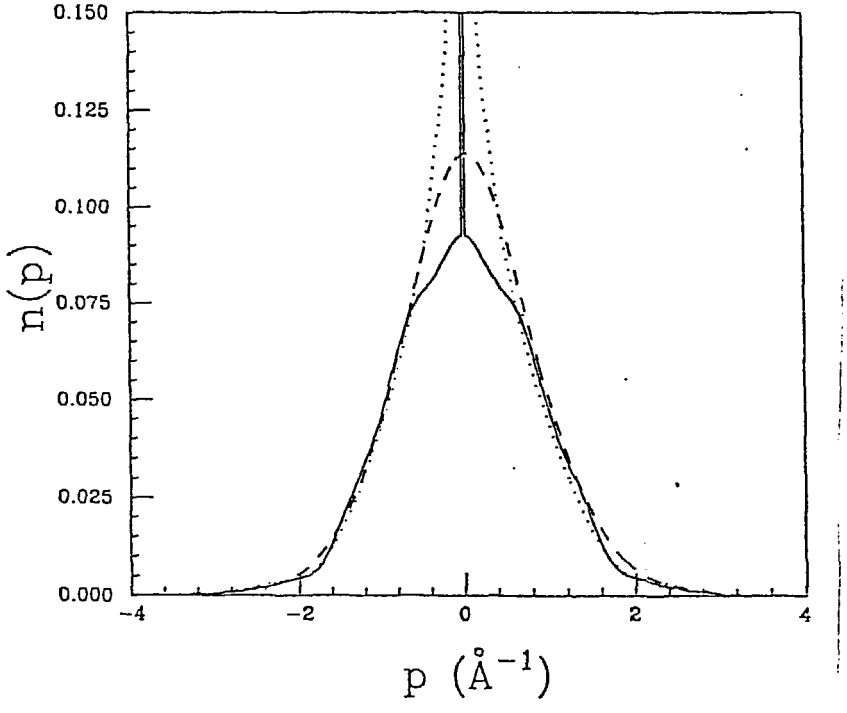


Fig. 1 Theoretical calculations of the momentum distribution. The ground state momentum distributions have been calcuated using GFMC[21] (solid) and variational[22] (dotted) techniques. The momentum distribution in the normal liquid (dashed) has been calculated using PIMC[23] techniques.

In a non-interacting gas, where the wavefunctions of the particles are free particle states and $p$ is a 'good' quantum number, $n_0$ is just the fraction of atoms in the zero momentum state. This is not true in the liquid where the interactions modify the states so that they are no longer free particle states and $p$ is no longer a 'good' quantum number. Every particle in the liquid now participates in the condensate and it is not appropriate to speak of a particular fraction of the atoms occupying the condensate, or $p = 0$ state. In the interacting liquid, the appearance of the condensate signals the development of off-diagonal long range order (ODLRO) at the one-particle level.[24,25] The condensate fraction is the magnitude of the microscopic order parameter for this phase.

The remainder of the momentum distribution, excluding the condensate $\delta$ function, is known as the uncondensed momentum distribution and exhibits several interesting features. At small $p$, which corresponds to long range interactions among the atoms, the effects of statistics are the dominant factor. For example, singular behavior[26,27] due to the coupling of the condensate to long wavelength collective excitations (phonons) appears. This singular behavior can be obtained exactly at small $p$ where the phonons are well defined and goes as $1/p^2$ in the ballistic regime and $1/p$ in the hydrodynamic regime. The variational $n(p)$ in Fig. 1 explicitly shows this behavior at small $p$. It is not present in the GFMC results, although this is presumably due to the relatively small size of the samples used in the numerical calculations. Alternately, the large $p$ behavior of $n(p)$ is determined primarily by the short range repulsive interaction between atoms and the statistics play little role.

The great majority of the numerical studies of the liquid have concentrated on the ground state due to the intrinsic limitations of the GFMC and variational approaches. However, Path Integral Monte Carlo (PIMC)[17] methods have recently been applied to study the liquid properties at finite temperatures. These calculations yield similar results to the ground state calculations at low temperatures i.e. a condensate fraction of approximately 9 %. However, they have the distinct advantage that they can provide results at finite temperature. For example, the condensate fraction can be obtained as a function of temperature where a rapid increase of $n_0$ is observed upon entering the superfluid with very little variation with temperature thereafter.

The momentum distribution may also be calculated in the normal liquid using PIMC. For example, Fig. 1 shows $n(p)$ at 3.33 K, well above the superfluid transition.[23] The momentum distribution is broad and featureless with a nearly Gaussian form, the familiar classical result. The width of the momentum distribution is determined by the quantum zero point motion of the liquid and is much larger than the width expected for classical particles. However, aside from this the shape of the momentum distribution in the normal liquid shows little effect due to quantum statistics.

## DEEP INELASTIC NEUTRON SCATTERING

Inelastic neutron scattering at large momentum transfer $Q$ provides the most direct means to obtain information on $n(p)$. In this limit, the scattering is due to single atoms and the final state of the scattering particle is assumed to be a free particle state. This is the well known Impulse Approximation (IA) and the observed scattering is proportional[15] to the Compton profile

$$J_{IA}(Y) = \frac{1}{4\rho\pi^2}\int_{|Y|}^{+\infty} pn(p)dp \qquad (3.1)$$

where $\rho$ is the density. The scattering in the IA does not depend on the energy and momentum transfer separately, but only through the scaling variable

$$Y \equiv (M/Q)(\omega - \omega_r) \qquad (3.2)$$

where $\omega$ and $Q$ are the energy and momentum transfer of the scattered neutron, M is the mass and $\omega_r = Q^2/2M$ is the recoil energy of the scattering atom.

In principle, the observed scattering at high $Q$ provides direct information on $n(p)$. However, in practice the momentum and energy transfers currently attainable are not sufficient to reach the IA limit. Deviations from the IA, due to interactions of the scattering particle with its neighbors, can significantly effect the scattering. These deviations are known as final state effects (FSE) since they modify the ideal plane wave final state of the scattering particle necessary for the application of the IA.

Final state effects have been the subject of several theoretical studies[2,28–41] and considerable controversy over both the form and the importance of FSE exists. Elsewhere in these proceedings[42] we present a detailed comparison of several theories for FSE in liquid helium. The comparison is limited to large Q's where the qualitative behavior is described by the IA. We find that, while several theories provide a good description of FSE in the normal liquid, most do not accurately describe FSE in the superfluid phase. However, we do find that one of the available theories seems to provide a good description of FSE in both the normal and superfluid phases. This theory, which is due to Silver, represents FSE as a convolution of a final state broadening function with the IA result for $J(Y)$. We shall use this theory later in comparisons of the theoretical predictions with the experimental results.

Ignoring, for the moment, the complications of FSE measurements of $J(Y)$ can be used to directly determine $n(p)$. For example, if $n(p)$ is Gaussian then $J(Y)$ is also a Gaussian with the same second moment. Furthermore, the condensate, which appears as the three-dimensional delta function in $n(p)$, is a one dimensional delta function in $J(Y)$.

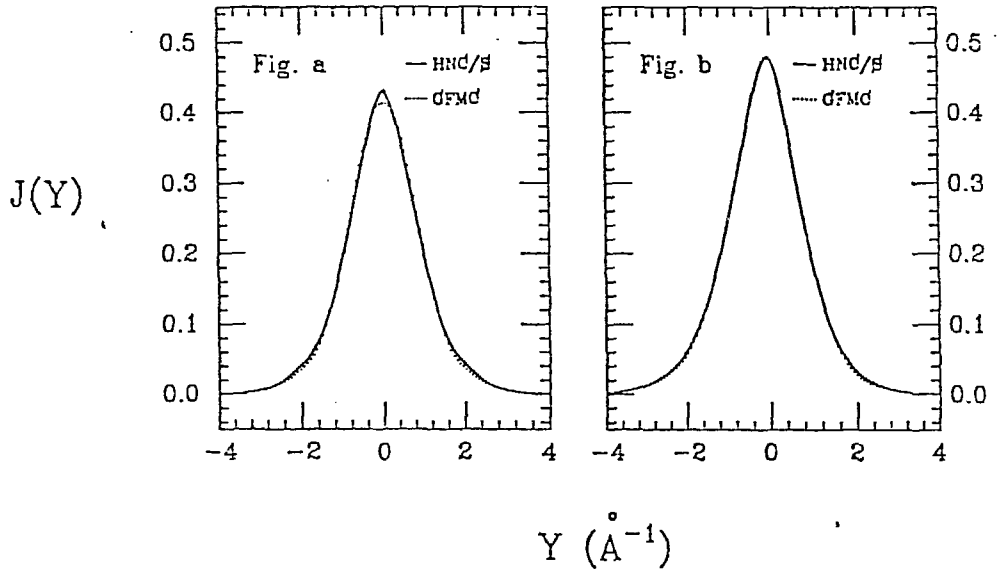


Fig. 2 Illustration of the relationship of $n(p)$ and $J(Y)$. a) shows the $J(Y)$ corresponding to the two ground state $n(p)$'s in Fig. 1. Both calculations have a condensate fraction of 9 %. However, the variational calculation (solid) shows the predicted $1/p$ singular behavior. This is lacking in the GFMC (dotted) result. b) shows the effect of instrumental resolution and FSE on the $J(Y)$ shown in a). The small differences between the predicted scattering for the two different calculations is now almost entirerly gone.

While there is a direct relationship between $J(Y)$ and $n(p)$, it is important to note that it is not a one-to-one correspondence. Features that are prominent in the momentum distribution may not be prominent in $J(Y)$. To illustrate this consider the two recent calculations of the ground state $n(p)$ discussed earlier and shown in Fig. 1. Both calculations predict a condensate fraction, which appears as a delta function with $n_0$=9.2 % . Both calculations also predict quite similar behavior at intermediate and large $p$. However, they differ markedly at small $p$. The variational calculation exhibits singular behavior due to coupling of long wavelength density fluctuations to the condensate which are not present in the GFMC result, presumably due to finite size effects in the calculation.

While $n(p)$ for these two calculations is quite different, the corresponding $J_{IA}(Y)$, shown in Fig. 2a, is remarkably similar. The singular behavior, which is the dominant feature in the variational $n(p)$ at small $p$, is quite small in $J(Y)$. When FSE and instrumental broadening are taken into account the (now small) differences between the predicted scattering for the two calculations all but disappear, as shown in Fig. 2b. The predictions of the two very different $n(p)$'s are now nearly indistinguishable! In principle, the differences between the two different $n(p)$'s we began with are still present in Fig. 2b. In practice, a measurement of the scattering would need fantastically good statistical accuracy to ever hope to observe these differences.

This insensitivity to the details at small $p$ is a direct consequence of the IA. The Compton profile, which is proportional to the measured scattering, is the momentum distribution in the direction of the momentum transfer, with the longitudinal components averaged over. Since this is the integral of $pn(p)$ features at small $p$, such as singular behavior, will be suppressed due to the $p$ in the integrand. Alternately, features at large $p$ will be enhanced, for exactly the same reason.

To further illustrate this point, consider the problem of extracting the momentum distribution from the observed scattering. The momentum distribution may be directly obtained form the observed scattering by inverting eq (3.1), which gives

$$n(p) = -\frac{1}{2\pi p}\frac{dJ(p)}{dp} \tag{3.3}$$

again neglecting the effects of instrumental resolution and FSE broadening. However, any experimental measurement will still be affected by the statistical uncertainty of the measurements. These statistical uncertainties will translate into uncertainties in the inferred $n(p)$, although the relative magnitude of the uncertainties will not be the same throughout the spectrum.

To illustrate the effects of statistics, consider the Gaussian $J(Y)$, obtained from a Gaussian $n(p)$, shown in Fig. 3a. Statistical noise, corresponding to a statistical accuracy of 3 % at the peak center, has been added. This is characteristic of the statistical accuracy obtained in typical neutron scattering studies. The momentum distribution is obtained from $J(Y)$ using eq (3.3), which requires a differentiation followed by a division by $p$. Fig. 3b shows the momentum distribution obtained from the data in Fig. 3a using a simple point by point differentiation procedure.

The most striking feature of the inferred momentum distribution is the increase in the statistical noise near $p = 0$, due to the division by $p$. This is the same effect observed previously when considering the shape of $J(Y)$ due to different $n(p)$'s. Even large differences in $n(p)$ at small $p$ may only cause small changes in $J(Y)$. Thus, the statistical noise present in $J(Y)$ allows a whole family of $n(p)$'s that are consistent with the observed data. This is reflected by the large errors in the inferred $n(p)$ near $p = 0$.

Admittedly, this has been an extreme example of the effects of inverting $J(Y)$ to obtain $n(p)$. Better (smoother) results can certainly be obtained by smoothing the data or using a more sophisticated differentiation procedure, but at the expense of

biasing the results. This example does, however, dramatically illustrate the difficulty in extracting the momentum distribution from the observed scattering.

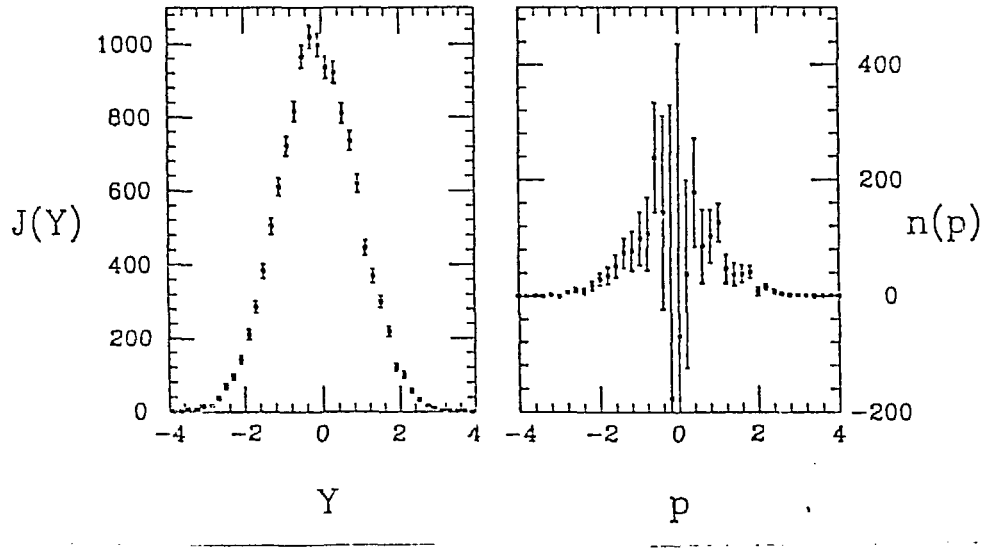


Fig. 3 a) $J(Y)$ obtained from a Gaussian $n(p)$ with statistical noise corresponding to 3 % at the peak added. b) $n(p)$ extracted from the scattering in a) using eq 3.3 using a simple point-by-pont differentiation. The errors are obtained from the statistical errors shown in a).

In view of the difficulties in extracting $n(p)$ from the experimental results, we find it more appropriate to work directly with $J(Y)$. Theoretical predictions can be compared to the experimental data using the IA, taking into account FSE and instrumental resolution. Working with $J(Y)$, as opposed to $n(p)$, has the distinct advantage that the statistical errors on the data provide a direct measure of the 'goodness-of-fit' between the theory and experiment.

## COMPARISON TO THEORY

Most previous measurements of liquid helium aimed at extracting information on $n(p)$ have been carried out using reactor based instruments[5−12] where the maximum momentum transfers obtainable, with reasonable resolution, are on the order of 5-15 $Å^{-1}$. Unfortunately, deviations from the IA predictions, such as asymmetry in the peak and oscillations in the width as $Q$ is varied, can still be quite significant at these $Q$'s. In addition, accurate theoretical descriptions of FSE, particularly in the superfluid, are lacking at these low $Q$'s.

In this review we will concentrate on recent measurements carried out using spallation neutron sources. These sources, with their high flux in the epithermal region, allow measurements at much larger $Q$'s with relative resolutions comparable to the lower $Q$ measurements at reactors. The higher $Q$'s have the advantage that the scattering is consistent with the predictions of the IA. In addition, FSE are more amenable to theoretical treatment at these higher $Q$'s.

To illustrate the results obtainable at spallation sources we will discuss recent measurements using the high resolution PHOENIX spectrometer at the Intense Pulsed Neutron Source, Argonne National Laboratory. Fig. 4 shows the measured

scattering at a $Q$ of 23 Å$^{-1}$, converted to $J(Y)$, at 4.2 K, in the normal liquid. The instrumental and final state broadening are also shown in Fig. 4 for reference. The instrumental resolution has been calculated using a Monte Carlo simulation of the instrument[43] and has been verified using measurements of low density helium gas. The final state broadening has been calculated by Silver for the $Q$ used in these measurements and is discussed in detail elsewhere.[30] The instrumental and final state broadening have similar widths and are both much less than the intrinsic width of the observed scattering. An accurate knowledge of these effects is essential if we hope to extract information on the underlying momentum distribution.

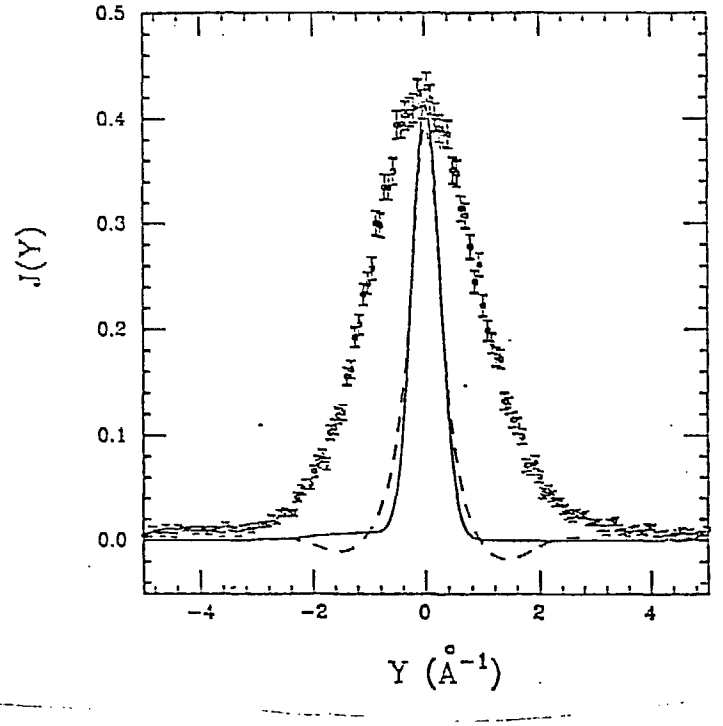


Fig. 4 The observed scattering, converted to $J(Y)$, at a $Q$ of 23 Å$^{-1}$ and a temperature of 4.2 K. The calculated instrumental resolution (solid line) and final state broadening (dashed line) are also shown.

The scattering shown in Fig. 4 is in qualitative agreement with the predictions of the IA. It is centered at and symmetric about $Y = 0$. In addition, measurements[44] at a variety of $Q$'s have shown that the shape of $J(Y)$ is independent of $Q$ above approximately 15 Å$^{-1}$. Thus, at least at this qualitative level the scattering is well described by the IA.

Fig. 5 shows the observed scattering at 3.5 K, in the normal liquid well above the superfluid transition, and 0.35 K, well below the superfluid transition. The scattering in both the normal liquid and the superfluid phase is broad and featureless. In the normal liquid, $J(Y)$ is nearly Gaussian, the classical result. In the superfluid, the scattering becomes visibly more peaked near $Y = 0$, but no distinct condensate peak is observed. This is consistent with the presence of a condensate peak broadened by instrumental resolution and FSE. However, due to the finite statistical accuracy of the results it is also consistent with a wide variety of momentum distributions, some which do not contain a condensate. Therefore, while the increase in scattering intensity at small $Y$ is indicative of a condensate, it does not provide any direct evidence for a condensate fraction.

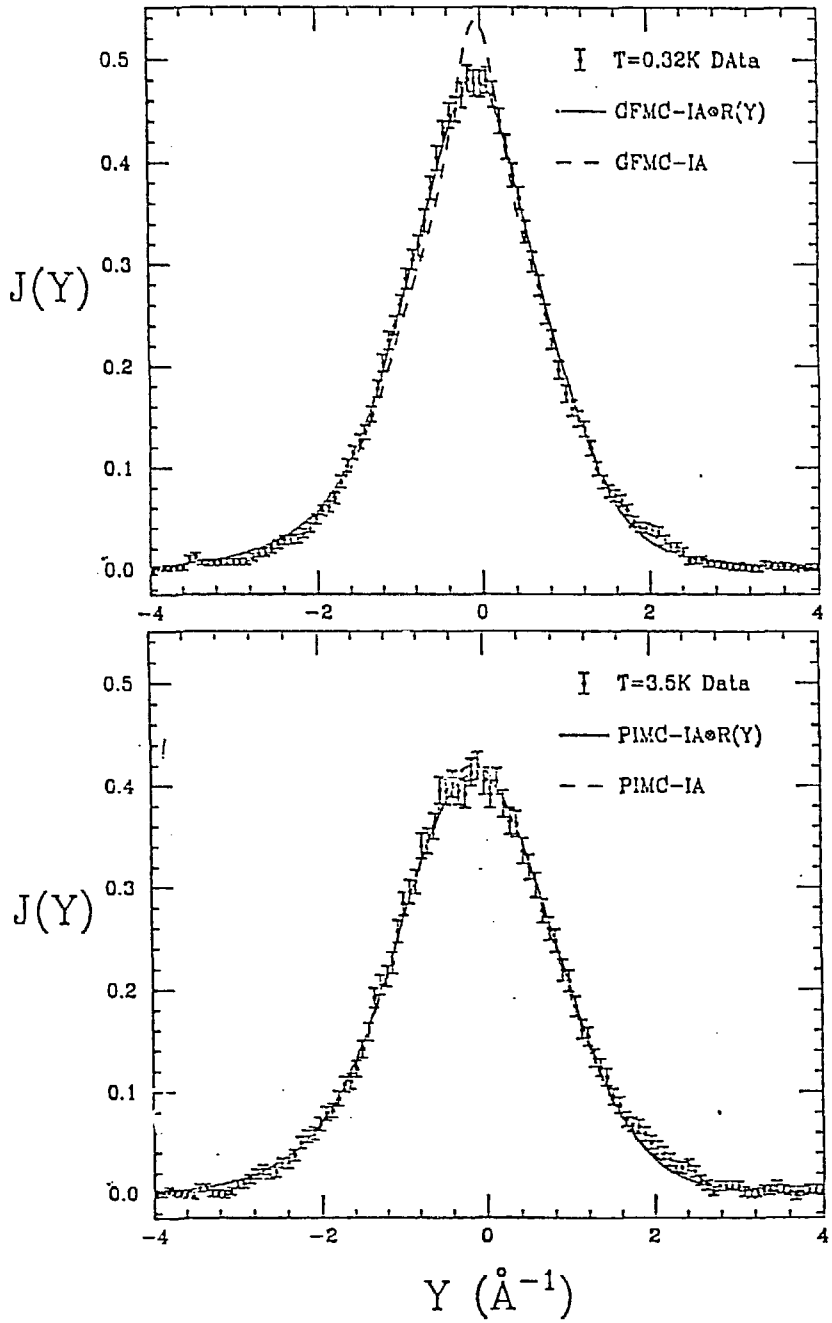


Fig. 5 The measured scattering in the normal liquid phase at 3.5 K (a) and the superfluid phase at 0.35 K (b) of liquid $^4$He. The dashed curves are the theoretical predictions for $n(p)$ transformed to $J(Y)$ and convoluted with instrumental resolution. PIMC calculations[23] at 3.33 K have been used for comparison with the normal liquid and are in excellent agreement with the experimental results. GFMC calculations[21] have been used for comparison with the superfluid and large discrepancies exist near $Y = 0$. The solid curves are again the theoretical predictions, but including the FSE broadening[30] shown in Fig. 4. The agreement between theory and experiment is now excellent in both the normal and superfluid phases.

The theoretical calculations of $n(p)$ may be compared with the experimental results, providing a direct test of the calculations. The dashed line in Fig. 5a shows the theoretical prediction for $J_{IA}(Y)$ in the normal liquid using the PIMC calculations[23,45] of $n(p)$. The theoretical $n(p)$ has been converted to $J(Y)$ using the IA and broadened by the instrumental resolution. The agreement between the theoretical predication and the experiment is excellent. In this case, direct application of the IA, using the theoretical $n(p)$, provides an excellent description of the scattering in the normal liquid. FSE have little effect on the observed scattering in the normal liquid at these $Q$'s.

The dashed line in Fig. 5b shows a similar comparison of the GFMC calculations[21] to the scattering in the superfluid. The agreement between the theoretical and experimental results is quite poor, particularly in the region of the peak center, where the condensate has the largest contribution. Based on this comparison, which has neglected FSE, we would conclude that the condensate fraction, if present at all, would have a much smaller value than the theoretical predictions.

Final state effects may be included by convoluting the theoretical predictions with the broadening function shown in Fig. 4. The solid lines in Fig. 5a and 5b are obtained when FSE are included. The predicted scattering in the normal liquid is changed very little by the inclusion of FSE. Certainly within the statistical accuracy of the measurement there is no observable change when FSE are included. Since, based on the $f^2$ sum rule, FSE do not change the second moment of the scattering they have little effect on the broad, nearly Gaussian $J(Y)$ in the normal liquid.

The change is much more dramatic in the superfluid phase where the momentum distribution has a sharp feature, the condensate. While FSE have little effect on the broad component of the scattering, as observed in the normal liquid, they significantly broaden the contribution from the condensate. Taking FSE into account, the agreement between theory and experiment is now excellent! For the first time *ab initio* calculations of $n(p)$ in the superfluid are in good agreement with experiment.

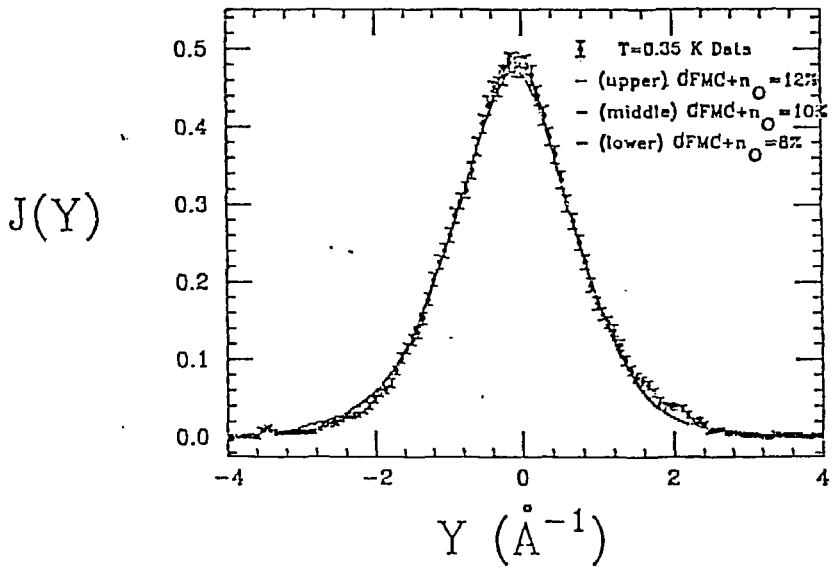


Fig. 6 Sensativity of the observed scattering to the magnitude of the condensate fraction at 0.35 K. GFMC calculations[21] have been used for the uncondensed component a narrow Gaussian to represent the condensate. The best agreement is obtained for $n_0$=10 % (central line). The two limiting values, $n_0$ = 8 and 12 % are the lower and upper lines, respectively.

An important point regarding the final state corrections is in order here. The final state broadening prediction of Silver, as shown in Fig. 4, has a narrow central peak and *negative* tails at high Y. The negative tails are essential if the broadening function is to satisfy the second moment sum rule. Thus, final state effects will not only broaden the condensate peak, they will also shift intensity around throughout the entire spectrum. For the particular FS broadening function used here, the negative tails will cause a *depletion* of the scattering at intermediate $Y$ when a condensate is present.

In view of the discussion in the previous section regarding the relationship between $J(Y)$ and $n(p)$ it is appropriate to examine how sensitive the observed scattering is to the theoretical $n(p)$. Inevitably there is a finite statistical accuracy attached to the experimental results and a whole range of different $n(p)$'s may give equally good agreement with the data. If the statistical accuracy of the results is high then only a limited range of $n(p)$'s, all with very similar shapes, will be consistent with the data. Alternately, if the statistical accuracy is poor then the experimental results will only place very weak constraints on the underlying shape of $n(p)$.

To illustrate this, consider the scattering in the superfluid phase shown in Fig. 5b. The theoretical $n(p)$ contains a very sharp feature, the condensate $\delta$ function. By replacing the condensate $\delta$ function with a Gaussian of variable width and amplitude we can obtain some measure of the sensitivity to this particular feature. The best agreement is obtained when the width of the Gaussian is less than 0.05 $\text{Å}^{-1}$ and $n_0$ is 10%, in agreement with the theoretical prediction for the condensate. Significant deviations are observed when the width is greater than 0.2 $\text{Å}^{-1}$ and $n_0$ is less than 8% or greater than 12%, as shown in Fig. 6. For this particular model for the uncondensed $n(p)$ provided by the GFMC calculation we find that there is indeed a condensate with $n_0 = 10 \pm 2$ %. However, we also point out that changing the shape of the uncondensed $n(p)$ could have an effect on the value for the condensate fraction.

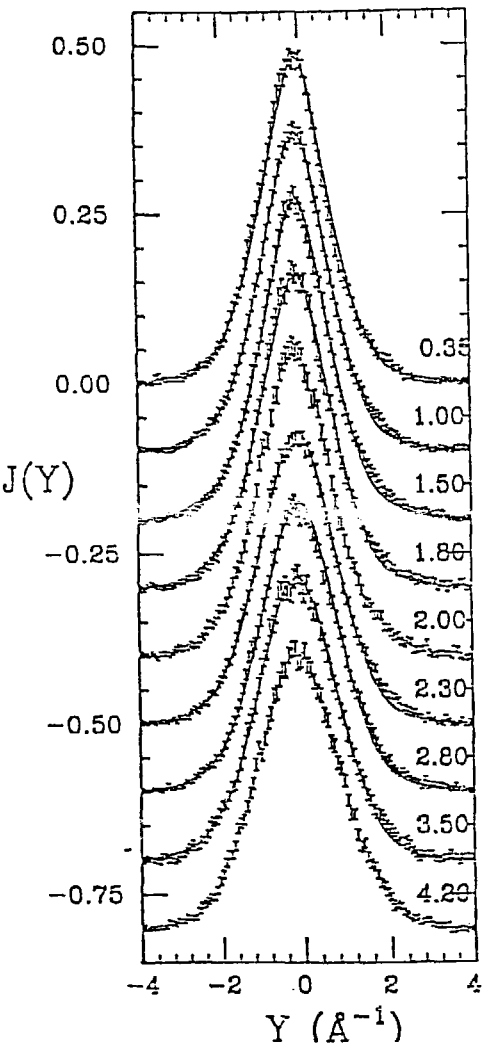


Fig. 7 Observed scattering at temperatures of 0.35, 1.0, 1.5, 1.8, 2.0, 2.3, 2.8, 3.5, and 4.2 K. The solid lines are the theoretical predictions with instrumental resolution and FSE included. GFMC calculations[21] are used for comparison with the 0.35 K results. PIMC calculations[45] are used for the remainder of the temperatures. No calculations are available for comparison with the 2.0 and 4.2 K measurements.

In a similar fashion, the sensitivity to the expected small $p$ singular behavior in $n(p)$ can be examined. The GFMC results, which give excellent agreement with the observed scattering, do not contain the expected singular contribution. The variational $n(p)$ discussed previously explicitly includes this behavior. However, a comparison of the observed scattering with the predictions of the variational calculation yields essentially the same results as for the GFMC calculation (see Fig. 2). This is not very surprising since the weak singular behavior at small $p$ is suppressed when $n(p)$ is transformed to $J(Y)$ as discussed earlier. Thus, the predicted small $p$ singular behavior makes little contribution to the observed scattering and, with the experimental techniques now available, will be difficult, if not impossible, to observe.

Thus, the experimental results in the superfluid provide a clear indication of a narrow component in $n(p)$ containing approximately 9-10 % of the intensity, which is very suggestive of the condensate. Unfortunately, due to the finite statistical error inherent in any experiment, they can not definitely prove the existence of a condensate, which is formally a $\delta$-function. Some other singular behavior, and not a condensate, could be responsible for the increase in the scattering at small $p$ observed in the superfluid. However, as seen in the comparison with the variational $n(p)$, this would have to be a very singular behavior, much more so than the $1/p$ singularity, to obtain agreement with the experimental results. Thus, while the experimental results can not rule out a ground state $n(p)$ which does not contain a condensate, they do provide strong evidence for a very narrow feature containing 10±2% of the total area. The excellent agreement with the theoretical predictions suggests that this very narrow feature is indeed the Bose condensate first predicted by London.[1]

To complete the comparison with the theoretical calculations, Fig. 7 shows measurements of the scattering from liquid helium at several temperatures between 0.35 K and 4.2 K. The solid lines in Fig. 7 are the theoretical predictions. The GFMC calculations[21] are used for comparison with the 0.35 K results, while the PIMC calculations[45] are used, where available, at temperatures above 1 K. The agreement is excellent over the entire temperature range! Theory and experiment appear to have converged for the momentum distribution in liquid $^4$He at low densities.

## EXTRACTION OF THE CONDENSATE FRACTION

Due to its importance in understanding the superfluid phase, considerable emphasis has been placed on determining the condensate fraction.[5-12,46-48] However, a direct determination of the condensate fraction has been frustrated by the failure to observe a distinct condensate peak. In addition, previous comparisons between the observed scattering and the theoretical predictions were not in agreement, and no value for the condensate could be inferred based on the theories. Therefore, alternate techniques to extract a value for the condensate fraction were developed. These all, in one form or another, involved modeling the momentum distribution in the superfluid to extract a value for the condensate fraction. A wide range of values for $n_0$ ( 2-17 % ) were obtained, depending on the particular model used. One central feature of all these models was that they implicitly assumed the condensate exists. Therefore, taking the pessimistic point of view, all the measurements can also be viewed as consistent with some increase in $n(p)$ at small $p$, but with no condensate.[49]

Due to the great emphasis that has been placed on extracting a value for $n_0$, as opposed to the overall shape of $n(p)$, we will examine this in detail. We will not attempt to review all the previous attempts to extract a value for the condensate fraction. Instead, we will examine one of these, due to Sears et al[46], which has been used in most recent measurements aimed at extracting the condensate.[9,10,44,46] Using this technique, values for the condensate fraction of ~ 10-13 % , when extrapolated to T=0, were originally obtained. These results were in resonable agreement with theoretical predictions. Recently, however, Griffin[50] pointed out that one of the central assumptions, regarding the changes induced in the uncondensed component of the momentum distribution, was incorrect. When the correct form for these changes

is used, the inferred values of $n_0$ are 4-5 % , considerably below the theoretical estimates.

Rather than review the previous measurements, over which there is some controversy, we will illustrate the basic ideas of this procedure by applying it to the measurements discussed earlier. We begin with the model for $n(p)$ in the superfluid phase. The momentum distribution may be written in the form

$$n(p,T) = n_0(T)\delta^3(p) + (1 - n_0(T))n^*(p,T) \tag{5.1}$$

where $\delta^3(p)$ represents the condensate, $n_0(T)$ is the condensate fraction, and $n^*(p,T)$ is the uncondensed component of the momentum distribution. The observed scattering in the superfluid phase, except near $Y = 0$, is quite similar to the scattering in the normal liquid. This suggests that the momentum distribution for the uncondensed component in the superfluid may be written in the form

$$n^*(p,T) = n(p,T_\lambda) \; + \; \frac{n_0(T)}{1 - n_0(T)}\delta n^*(p,T) \; ) \tag{5.2}$$

where $n(p,T_\lambda)$ is the normalized momentum distribution in the normal liquid and $\delta n^*(p,T)$ represents changes in the uncondensed $n(p)$ below $T_\lambda$.

In the absence of FSE and instrumental resolution, measurement of $J(Y)$ would provide a direct observation of the condensate. However, in the presence of these effects the condensate $\delta$-function will be broadened. In practice, the broadening is sufficiently large the condensate peak is no longer resolved from the uncondensed component.

While, no distinct condensate peak is observed, the effects of the condensate will still be present in the observed scattering. In general, they will appear as an increase in the scattering near $p = 0$, rather than a distinct peak. The condensate fraction may then be extracted from the observed scattering in the superfluid under two assumptions. They are:

- The entire contribution of the condensate peak occurs within some small region around $Y = 0$.
- The changes in the uncondensed momentum distribution can be accounted for using theoretical calculations.

From the first assumption the scattering due to the condensate will only contribute in the region around $Y = 0$. In terms of $n(p)$, the total intensity in a region within $p_c$ of the origin is

$$\alpha(T,p_c) = \int_0^{p_c} n(T,\vec{p})\; d\vec{p} \; . \tag{5.3}$$

Since this region, by assumption, contains the entire contribution of the condensate we find

$$n_0(T,p_c) = \frac{\alpha(T,p_c) - \alpha(T_\lambda,p_c)}{1 - \alpha(T_\lambda,p_c) + \gamma} \tag{5.4}$$

where

$$\gamma = \int_0^{p_c} \delta n^*(p,T)\; 4\pi p^2 dp \tag{5.5}$$

Thus, knowing the form of $\delta n^*(p)$ in the region within $p_c$, which is where the modeling of $n(p)$ enters, we can directly obtain the condensate fraction.

One of the central assumptions in the derivation of (5.4) is that the entire contribution of the condensate is confined to the region around the origin. Instrumental

resolution, which broadens the condensate peak, certainly satisfies this requirement. However, FSE are a different matter. As shown in the last section, they not only broaden the peak but they shift intensity from one part of the spectrum to another. This certainly violates the assumption above that the condensate contribution is still localized around the origin.

Final state effects must, at least in part, be taken into account if we hope to determine $n_0$. The most important feature of FSE to account for is the shifting of intensity caused by the final state broadening. This may be accomplished by deconvoluting the final state broadening function used earlier from the observed scattering. While, due to the statistical noise in the results, this will not entirely remove FSE it should at least account for the major effects.

Rather than attempt a numerical deconvolution, a difficult and unstable procedure with statistically noisy data, we have found it convenient to represent the scattering by a functional form and then fit this form, convoluted with instrumental resolution and FSE, to the observed scattering. A model consisting of two Gaussians, with variable amplitudes and widths and a center fixed at $Y = 0$, provides sufficient freedom to fit the data in the normal and superfluid phases. This model has the advantage that certain physical constraints, such as symmetry, positivity, etc, are implicitly included in the results of the deconvolution.

The results of deconvoluting FSE and instrumental broadening from the observed scattering are shown in Fig. 8. At high temperatures, near 4K, the scattering is nearly Gaussian. However, as the temperature is lowered toward $T_\lambda$ the scattering becomes more peaked near $Y = 0$, even in the normal liquid. A large increase in the scattering intensity at small $Y$ is observed at $T_\lambda$. The scattering in the superfluid becomes much more peaked, indicating the presence of a condensate.

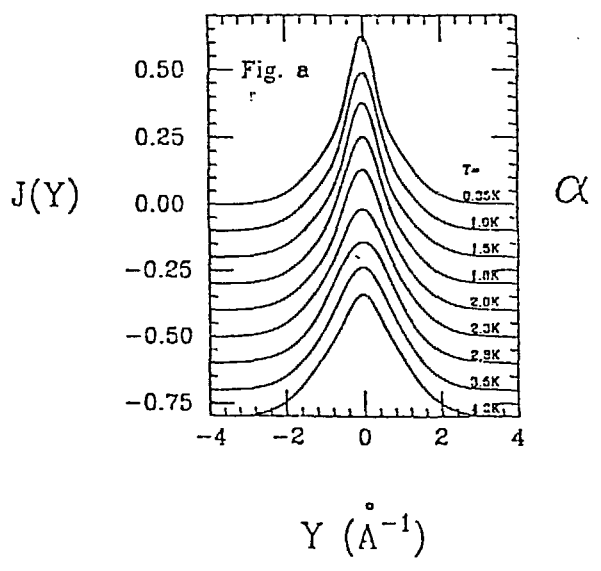


Fig. 8 Observed scattering of Fig. 7 with instrumental resolution and FSE effects removed as described in the text.

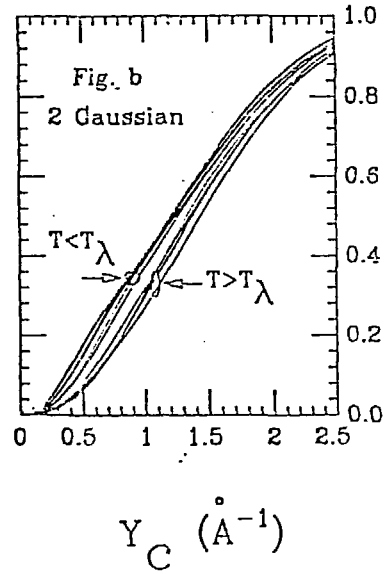


Fig. 9 Integrated scattering from 0 to $p_c$ using the scattering shown in Fig 8. The gap between the results above and below the superfluid transition is indicative of the formation of a condensate.

While the sharp increase in the scattering intensity at small $p$ in the superfluid is consistent with the presence of a condensate, again no $\delta$ function appears in the deconvolutions in the superfluid phase. However, these same results were in excellent agreement with the theoretical predictions containing a condensate. Thus, the lack of a distinct condensate peak in the results is a direct consequence of the statistical noise present in the data. In fact, due to the statistical noise in the data, a whole series of $n(p)$'s are consistent with the results, including those with $\delta$ functions as show earlier (Fig. 5b). Thus we take the width of the narrow component in the fits, which is $\sim 0.6$ Å$^{-1}$, as indicative of the statistical smearing of the condensate peak.

In previous measurements at lower $Q$'s, FSE are quite significant and the IA is not even qualitatively satisfied. No detailed theories for FSE are available at these lower $Q$'s and approximate techniques such as symmetrization and averaging over different $Q$'s have been used to remove the deviations from the IA.[9,10,46] However, as we show elsewhere in these proceedings,[42] these procedures do not properly account for the shifting of intensity by FSE. Therefore, the increase in scattering at $p$ can not be uniquely identified with the contribution from the condensate, violating one of the central assumptions used.

The integrated intensity, $\alpha$, may be obtained directly from the results in Fig. 8 using a simple integration by parts of (5.3). Fig. 9 shows $\alpha(p_c, T)$ versus $p_c$ and T in both the normal and superfluid phases. The most prominent feature is the gap between the curves for the normal and superfluid between 0.5 and 1.5 Å$^{-1}$. The appearance of this gap is a dramatic signal of the formation of the Bose condensate and the size of the gap is proportional to the condensate fraction.

Changes in the uncondensed $n(p)$ due to the presence of the condensate also contribute to the scattering at small $p$ and must be taken into account if $n_0$ is to be determined. These cannot be experimentally separated from the condensate contribution and we must make recourse to the theoretical predictions for the small $p$ behavior. The main condensate induced change, at small $p$, is the singular behavior introduced by fluctuations in the condensate coupling to long wavelength density fluctuations (phonons). The form for the small $p$ singular behavior[26,27,50] is

$$\begin{aligned} \delta n(p,T) &= \frac{mk_BT}{(2\pi)^3\hbar^2\rho n_s}\ \frac{1}{p^2} \qquad p < \frac{k_BT}{\hbar c} \\ &= \frac{mc}{2(2\pi)^3\hbar\rho}\ \frac{1}{p} \qquad p < \frac{k_BT}{\hbar c} \end{aligned} \tag{5.6}$$

where $\rho$ is the density, $n_s$ is the superfluid fraction, and $c$ is the velocity of sound. Griffin[50] has pointed out that the crossover between these two regimes takes place at small $p$ ($k_BT/\hbar c$ is only .1 Å$^{-1}$ at 2 K) so that the contribution of the $1/p^2$ term is negligible. Therefore, in the phonon region ($p <\sim 0.7$ Å$^{-1}$) where this result should be valid, $\gamma$ is then $0.85n_0p^2$. In addition, Griffin[50] has attempted to extend this result beyond the phonon region using the measured dispersion relation, assuming the $1/p$ singular behavior is still valid.

The condensate fraction can be obtained directly from the results in Fig. 9 using the theoretical predictions for the condensate induced changes. Fig. 10 shows the condensate fraction, using Griffin's[50] calculation of $\gamma$ as a function of $p_c$. Ideally, if instrumental resolution and FSE were absent and if $\delta n^*(p,T)$ were correct, the condensate fraction would be a constant, independent of $p_c$. The experimental results differ significantly from this expectation.

The inferred $n_0$ start at zero when $p_c = 0$, increase to a maximum value in the range of 0.6 to 0.8 Å$^{-1}$, and then decreases again to zero. The behavior near $p_c = 0$ is not surprising since there is no $\delta$ function singularity in the two Gaussian fits that would give a rapid rise at $p = 0$. The width of 0.6 Å$^{-1}$ is just the statistical

broadening associated with the condensate peak in the deconvolutions. We would not expect the results to be valid for $p_c$ less than this value. The decrease at large $p_c$ is also not surprising since the scattering in the normal and superfluid phase is almost identical in this region.

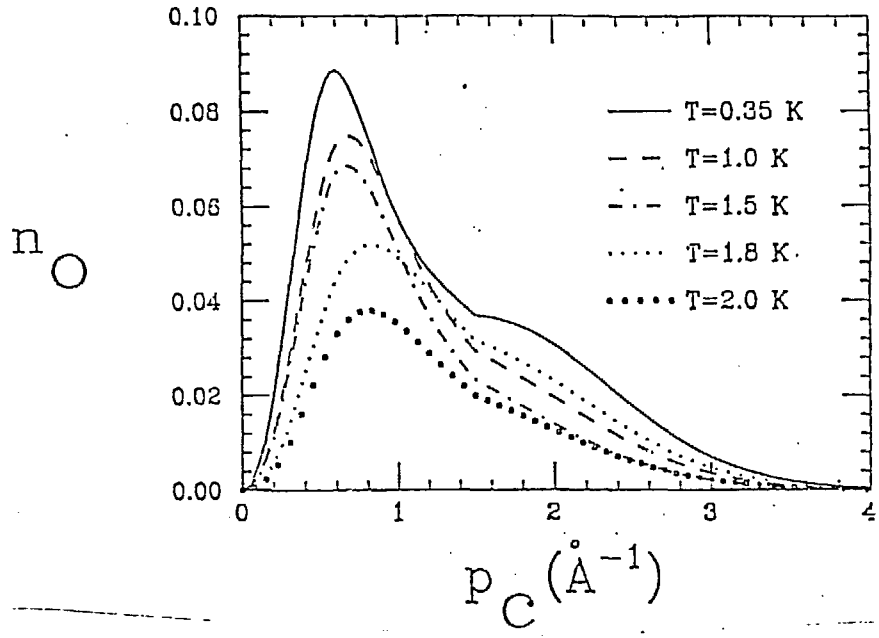


Fig. 10 Inferred values of the condensate fraction at temperatures of 0.35, 1.0, 1.5, 1.8, and 2.0 K. The curves are described in the text.

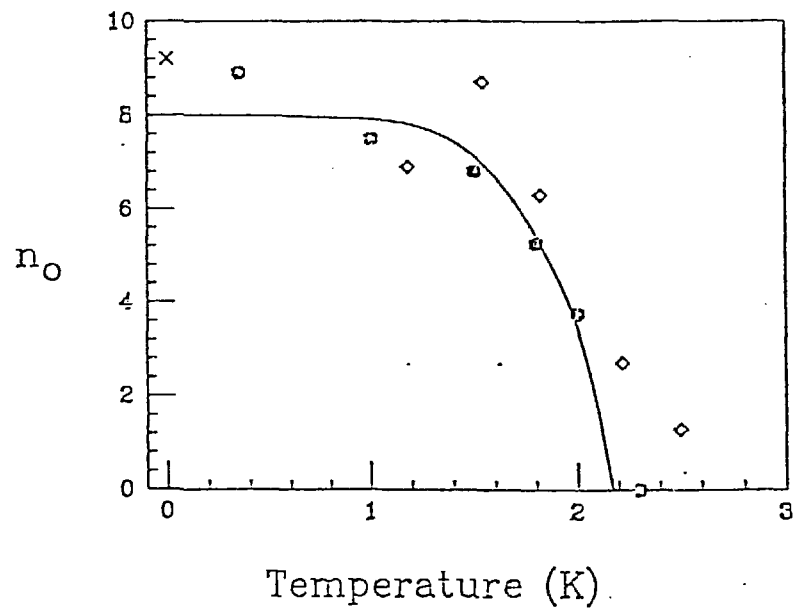


Fig. 12 Maximum of the inferred $n_0$ versus temperature (heavy dots). Also shown are the GFMC (cross) and PIMC (diamonds) results. The curve is a fit to the data with a critical exponent of 6 as described in the text.

There is a further limitation on the values of $p_c$ appropriate for the extraction of $n_0$. The theoretical correction for the condensate induced changes $\gamma$ is only valid within the phonon region, which extends to $\sim$ 0.8 $\AA^{-1}$. Above this region, the behavior of the condensate induced corrections have only been extrapolated. Thus, above $\sim$ 0.8 $\AA^{-1}$ the model for the condensate induced changes is suspect.

This is precisely the region where the broad maximum in the inferred condensate occurs. Thus, we use the peak values for $n_0$ as a function of $p_c$ as representative of the condensate fraction in the liquid. These values are shown in Fig. 11. At low temperatures, the inferred $n_0$ is $\sim$ 10 % , in good agreement with the GFMC and variational results. In addition, the inferred $n_0$, shows a slow decrease with increasing temperature followed by a rapid drop at the superfluid transition, consistent with the rapid depletion near the superfluid transition predicted by PIMC studies.

Finally, we note that most previous attempts to extract the condensate[46] a different form for the small $p$ changes in $n(p)$ has been used. This lead to values of the condensate on the order of 10-13 % at T=0, in reasonable agreement with theory. However, Griffin[50] pointed out that this form was based on an incorrect combination of the two limiting behaviors shown above. When the correct form for the small $p$ singular behavior is used values of 4-5 % at T=0 are obtained.

The temperature dependence of the condensate fraction has often been characterized by fitting to a form such as

$$n_0(T) = n_0(0)[1 - (T/T_\lambda)^\alpha] \tag{5.7}$$

where $n_0(0)$ is the limiting value of the condensate fraction at T+) and $\alpha$ is a critical exponent. Past measurements have found $\alpha$ on the order of 3.6, indicating a fairly weak temperature dependence. However, these values were based on the incorrect form of the small $p$ behavior of the condensate induced changes. The solid curve in fig. 12 is a fit to the results here and gives $n_0 = 8.0\%$ and $\alpha = 6$. The larger value of reflects a much sharper temperature dependence than previously reported. As can be seen in the figure, the condensate exhibits little temperature dependence until quite near $T_\lambda$ and then drops quite rapidly.

In summary, it appears that resonable values for the condensate fraction in the superfluid phase can be extracted using techniques such as these. However, it is essential that both FSE broadening be properly taken into account and that a good theoretical model for the condensate induced changes be available. The values obtained for $n_0$ will be valid only to the extent that both these conditions are satisfied.

## CONCLUSIONS

We have now reached a stage where there is excellent agreement between the theoretical results and the experimental observations for all aspects of the momentum distribution in liquid $^4$He. In particular, the agreement between theory and experiment settles the long-standing question regarding the magnitude, and even the presence, of a Bose condensate in the superfluid. The experimental results provide convincing evidence for a Bose condensate containing 10 % of the atoms.

This recent convergence of theory and experiment has come about through several simultaneous advances. Theoretically, the availability of more powerful computational techniques and facilities for the calculation of $n(p)$ has lead to very accurate theoretical predictions. In addition, the development of accurate theoretical predictions for the FSE broadening, particularly in the superfluid, has allowed *ab initio* comparisons of the theoretical and experimental results. Experimentally, the development of spallation sources has allowed us to obtain high quality results with good statistical accuracy.

A better understanding of the strengths and weakness's of DINS as applied to determinations of $n(p)$ in quantum systems has also evolved. For example, the insensitivity of the observed scattering to some of the singular behavior in $n(p)$ is now

understood. We have tried to convey an appreciation of where the measurements can provide a definite test of theories and where they are not sensitive to particular details.

Unfortunately, the original goal for much of the work in liquid helium, a direct observation of the condensate fraction, has not come to pass. In view of our current understanding of FSE in helium, it is unlikely that this goal will ever be reached in deep inelastic neutron scattering experiments. While the current experimental results do not definitively prove the existence of a condensate, they do provide such overwhelming evidence that we can now consider the problem, for the bulk liquid at least, solved.

We would like to acknowledge useful discussions with R.N. Silver, H.R. Glyde, D.L. Price, C.K. Loong, P.A. Whitlock, and R.M. Panoff. This work was supported by the National Science Foundation under grant DMR-8704288 and by OBES/DMS support of the Intense Pulsed Neutron Source at Argonne National Laboratory under DOE grant W-31-109-ENG-38.

References

1 F. London, Nature 141, 643 (1938).
2 P.C. Hohenberg and P.M. Platzman, Phys. Rev. 152, 198 (1966).
3 for reviews see E. C. Svensson, V.F. Sears, Physics 137B, 126 (1986.)
4 H. Mook, contribution in these procedings.
5 R.A. Cowley and A.D.B. Woods, Phys. Rev. Lett. 21, 787 (1968).
6 R.A. Cowley and A.D.B. Woods, Can. J. Phys. 49, 177 (1971).
7 P. Martel, E.C. Svensson, A.D.B. Woods, V.F. Sears, and R.A. Cowly, J. Low Temp. Phys. 23, 285 (1976).
8 H.A. Mook, Phys. Rev. Lett. 32, 1167 (1974).
9 H.A. Mook, Phys. Rev. Lett. 51, 1454 (1983).
10 H.A. Mook, Phys. Rev. B 37, 5806 (1988).
11 E.C. Svensson, V.F. Sears, A.D.B. Woods and P. Martel, Phys. Rev. B 21, 3638 (1980); V.F. Sears, E.C. Svensson, A.D.B. Woods and P. Martel, Atomic Energy of Canada Limited Report No. AECL-6779 (unpublished).
12 A.D.B. Woods and V.F. Sears, Phys. Rev. Lett. 39, 415 (1977).
13 H.R. Glyde and E.C. Svensson in Methods in Experimental Physics, Vol. 23B, D.L. Price and K. Sköld, ed. Academic Press, 1987 p.303.
14 V.F. Sears, Can. J. Phys. 63, 68 (1985).
15 P.E. Sokol, R.N. Silver, and J.W. Clark, contribution in these proceedings.
16 E. Manousakis, contribution in these procedings.
17 D.M. Ceperley, contribution in these procedings.
18 R. Panoff and P. Whitlock, contribution in these procedings.
19 J.W. Clark and M.L. Ristig, contribution in these proceedings.
20 A. Griffin, Can. J. Phys. 65, 1368 (1987).
21 P.A. Whitlock and R. Panoff, Can. J. Phys. 65, 1409 (1987).
22 E. Manousakis, V. R. Pandharipande, Q. N. Usmani, Physical Review B 31, 7022 (1985); E. Manousakis, V. R. Pandharipande, ibid., 7029.
23 D.M.Ceperly and E.L.Pollock, Phys. Rev. Lett. 56, 351 (1986).
24 O. Penrose and L. Onsager, Phys. Rev. 104, 576 (1956).
25 C.N. Yang, Rev. Mod. Phys. B34, 694 (1962).
26 P.C. Hohenburg and P.C. Martin, Ann. Phys. (N.Y.) 34, 291 (1965).
27 J. Gavoret and P. Nozières, Ann. Phys. (N.Y.) 28, 349 (1964).
28 R.N. Silver, contribution in these proceedings.
29 H.R. Glyde and W. Sterling, contribution in these proceedings.
30 R. N. Silver, in Proceedings of the 11th International Workshop on Condensed Matter Theories, Oulu, Finland, 1987, Plenum Press; Rapid Communications,

Physical Review B, March 1 (1988).
31 P.M. Platzman and N. Tzoar, Phys. Rev. B 30, 6397 (1984).
32 H.A. Gersch, and L.J. Rodriguez, Phys. Rev. A 8, 905 (1973); L.J. Rodriguez, H.A. Gersch and H.A. Mook, ibid. 9, 2085 (1974.)
33 T.R. Kirkpatrick, Phys. Rev. B 30, 1266 (1984).
34 G. Reiter and T. Becher, Phys. Rev. B 32, 4492 (1985).
35 J.J. Weinstein and J.W. Negele, Phys. Rev. Lett. 49, 1016 (1982).
36 W.C. Kerr, K.N. Pathak and K.S. Singwi, Phys. Rev. A 2, 2416 (1970).
37 P. Martel, E.C. Svensson, A.D.B. Woods, V.F. Sears, and R.A. Cowly, J. Low Temp. Phys. 23, 285 (1976).
38 A.S. Rinat, Phys. Rev. B 36, 5171 (1987).
39 V.F. Sears, Phys. Rev. B 30, 44 (1984).
40 S. Stringari, Phys. Rev. B 35, 2038 (1987).
41 B. Tanatar, G.C. Lefever, and H.R. Glyde, J. Low Temp. 62, 489 (1986).
42 P.E. Sokol, T.R. Sosnick, W.M. Snow, and R.N. Silver, Contribution in these proceedings.
43 P.E. Sokol, G.K. Kellogg, W.M. Snow, T.R. Sosnick, and J.M. Carpenter, to be published.
44 P.E. Sokol, Can. J. Phys. 65, 1393 (1987).
45 D.M. Ceperly, and E.L. Pollock, Can. J. Phys. 65, 1416 (1987).
46 V.F. Sears, E.C. Svensson, P. Martel and A.D.B. Woods, Phys. Rev. Lett. 49, 279 (1982).
47 O.K. Harling, Phys. Rev. A 3, 1073, (1971), A.G. Gibbs and O.K. Harling, *ibid.* 7, 1748, (1973).
48 H.A. Mook, R Scherm, and M.K. Wilkinson, Phys. Rev. A 6, 2268 (1972).
49 H. W. Jackson, Phys. Rev. A 10, 278 (1974).
50 A. Griffin, Phys. Rev. B 32, 3289 (1985).

## DISCLAIMER